EBSD-assisted fractographic analysis of crack paths in magnesium alloy

S. Takaya
Graduate School of Engineering, Gifu University, Japan

Y. Uematsu, T. Kakiuchi
Faculty of Engineering, Gifu University, Japan
yuematsu@gifu-u.ac.jp

ABSTRACT. Magnesium (Mg) alloys are attractive as structural materials due to their light weight and high specific strength. It is well known that Mg alloy has hexagonal close-packed (HCP) structure and only basal slip or twinning can operate during plastic deformation because critical resolved shear stresses of the other slip systems such as pyramidal or prismatic slips are much higher than the basal slip. Thus sometimes characteristic fracture surfaces are formed during stress corrosion cracking (SCC) or fatigue crack propagation (FCP) in Mg alloys, where many parallel lines are formed. These lines are different from so-called fatigue striations, because they are formed even under sustained load condition of SCC. Consequently, electron back scattered diffraction (EBSD) technique was applied on the fracture surface, and the formation mechanism of parallel lines was investigated. EBSD-assisted fractography had revealed that the characteristic parallel lines were formed due to the operation of basal slips, not twining. It is considered that hydrogen-enhanced localized plasticity (HELP) mechanism had been activated under corrosive environment.

KEYWORDS. EBSD-assisted fractography; Magnesium alloy; Fatigue crack propagation; Stress corrosion cracking; Corrosive environment.

INTRODUCTION

Magnesium (Mg) alloys draw attention as light weight structural material because of light weight and high specific strength. To use Mg alloys for mechanical components, it is important to understand mechanical properties, such as fatigue strength and fatigue crack propagation (FCP) resistance. In addition, it is well known that the resistance of Mg alloys against corrosion is low comparing with other light weight alloys. Consequently, stress corrosion cracking (SCC) [1-5] and FCP [6, 7] behaviors under corrosive environment should be understood. The authors had performed SCC tests using AZ31 and AZ61 Mg alloys [4, 5], and indicated that crack propagation rates were faster in AZ31 than in AZ61. The fractographic analyses revealed that characteristic fracture surfaces were formed in which many parallel lines were recognized within grains. Furthermore, the authors had conducted FCP tests [6, 7] using T5-treated AZ61 under corrosive conditions and dry air, showing that FCP rates were accelerated by hydrogen diffusion near the crack tip [7]. The parallel lines were formed under corrosive conditions similar to SCC fracture surfaces, which were different from so-called fatigue striations. Such parallel lines were not so prominent on the fracture surfaces of FCP in dry

air without corrosion [7]. Fig. 1(a), (b) and (c) show typical fracture surfaces in SCC [5], FCP in corrosive environment and in dry air [6. 7], respectively. It should be noted that parallel lines are recognized under SCC and FCP in corrosive environment, while not under FCP in dry air.

Mg alloy has hexagonal close-packed (HCP) structure, and it is known that only basal slip or twinning can operate during plastic deformation. That is because critical resolved shear stresses (CRSS) of the other slip systems such as pyramidal or prismatic slips are much higher than the basal slip. The characteristic plastic deformation behavior would be related to the formation of parallel lines on SCC or FCP fracture surfaces. However, the formation mechanism of parallel lines is not clear from crystallographic point of view. In the present study, electron back scattered diffraction (EBSD) technique was applied directly on the fracture surface, and the formation mechanism of parallel lines was discussed based on the EBSD-assisted fractography.

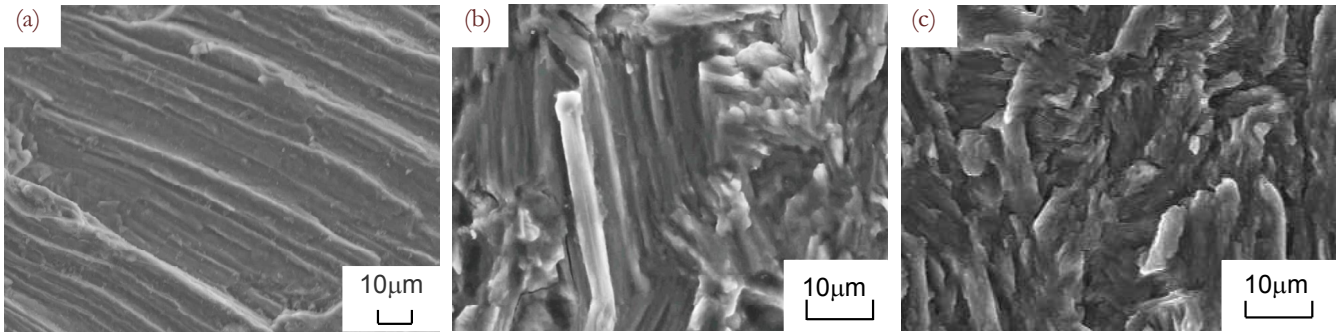

Figure 1: Typical fracture surfaces; (a) SCC under -1.4V cathodic potential, (b) FCP under -5V cathodic potential, (c) FCP in dry air.

EXPERIMENTAL PROCEDURE

The material used is T5-treated AZ61 cast Al alloy. The chemical composition (wt. %) is as follows, Al: 6, Zn: 0.67, Mn: 0.34, Si: 0.01, Cu: 0.002, Ni: 0.001, Fe: 0.004, Mg: balance. All SCC and FCP tests were performed using compact tensiotn (CT) specimen in accordance with ASTM E647. The detailed information of SCC and FCP test procedures is in the references [4, 5] and [6, 7], respectively.

EBSD assisted fractography was performed by the following procedure. As schematically shown in Fig.2, when characteristic parallel lines are found on the fracture surface by SEM, small Vickers indentations are put near the lines. Subsequently, the fracture surface was polished by buffing followed by ion milling. The depth of polishing was identified from the change of the size in Vickers indentation. In all cases, the depth was identified as 10-20 μm. EBSD analysis gives Euler angle of each grain. Schmid factors and the angles of slip lines on the specimen surfaces were calculated from Euler angles.

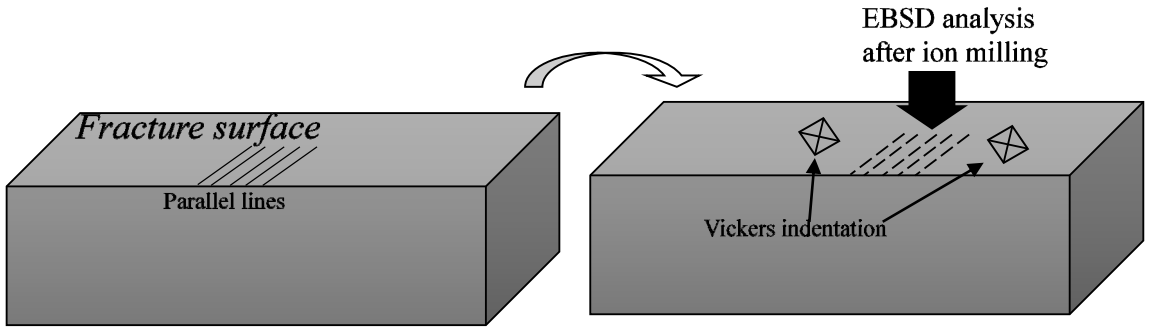

Figure 2: Schematic illustration of EBSD assisted fractography procedure.

RESULTS AND DISCUSSION

Stress corrosion cracking (SCC) under the cathodic potential of -1.4V

Fig. 3 shows the fracture surfaces of SCC test under the cathodic potential of -1.4V [5]. Fig. 3(b) is the magnified view of fracture surface at K =23.7MPam$^{1/2}$. It should be noted that parallel lines are recognized near the edge of specimen surface. As shown in Fig.3(c), the areas with parallel lines are classified into three areas, I, II and III. The angle between the parallel lines and horizontal line was 89º, 65º and 80º for the area I, II and III, respectively. Vickers indentations were put around the lines (see Fig.4(a)) and the change of the size of Vickers indentation before and after polishing gave the depth of polishing around 10 to 20 μm.

Fig. 5(a), (b) and (c) show the EBSD analytical results in the areas I, II and III, respectively. Due to the limitation of the polishing depth, low CI (Confidence Index) value area is relatively wide in all observations. But the grain orientations in all figures are identified from the areas with high CI values. First, it should be noted that twining was not found in all areas.

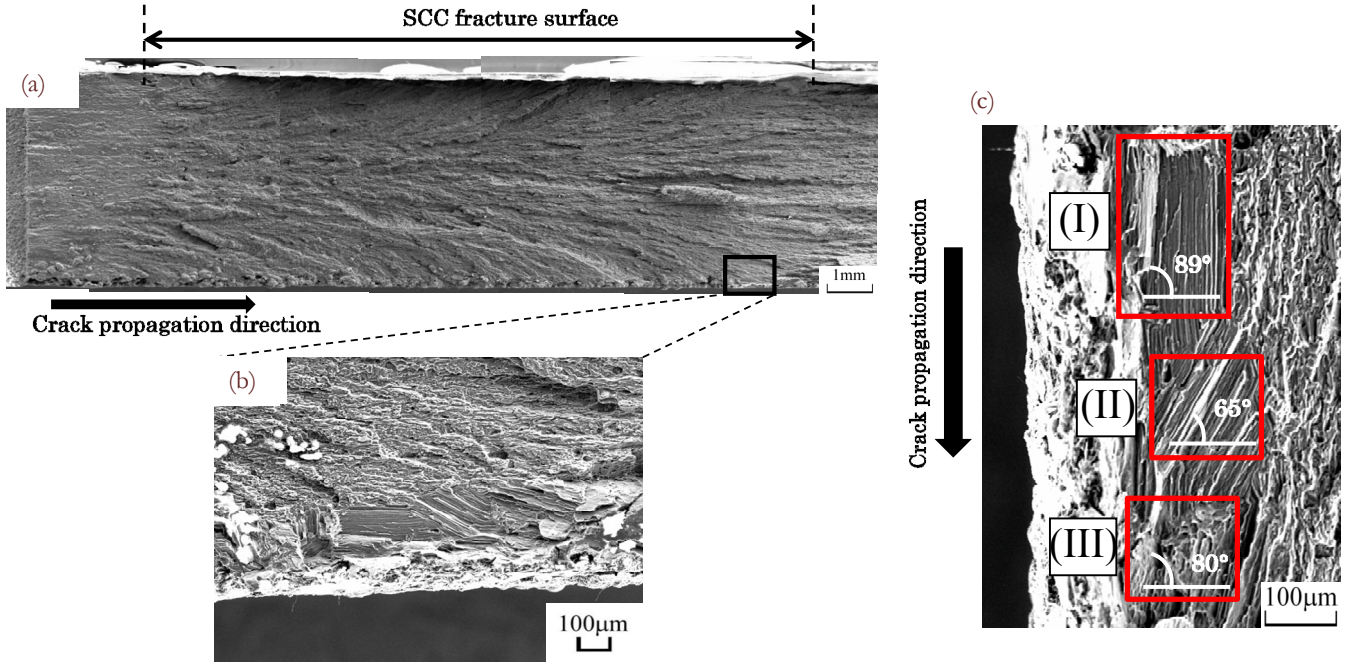

Figure 3: SEM micrographs showing SCC fracture surface tested under the cathodic potential of -1.4V; (a) Macroscopic appearance, (b) Magnified view showing parallel lines, (c) Classification of the areas with parallel lines.

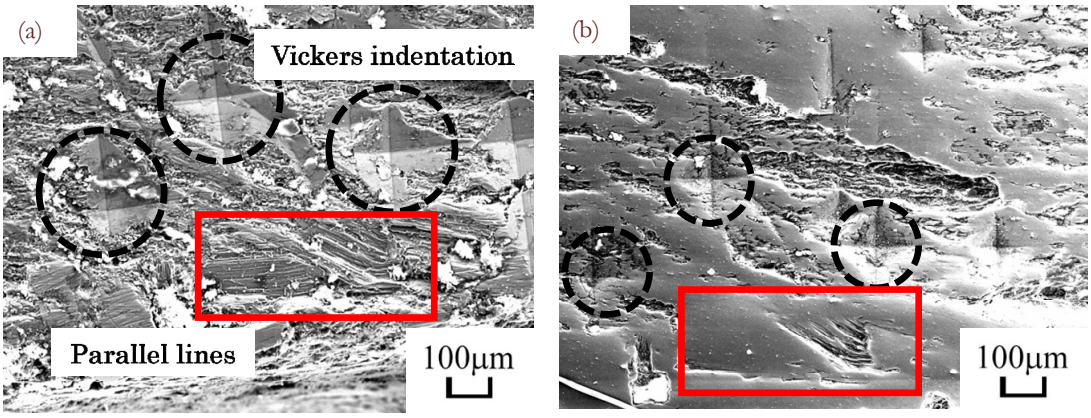

Figure 4: Vickers indentation around parallel lines; (a) Before polishing, (b) After polishing.

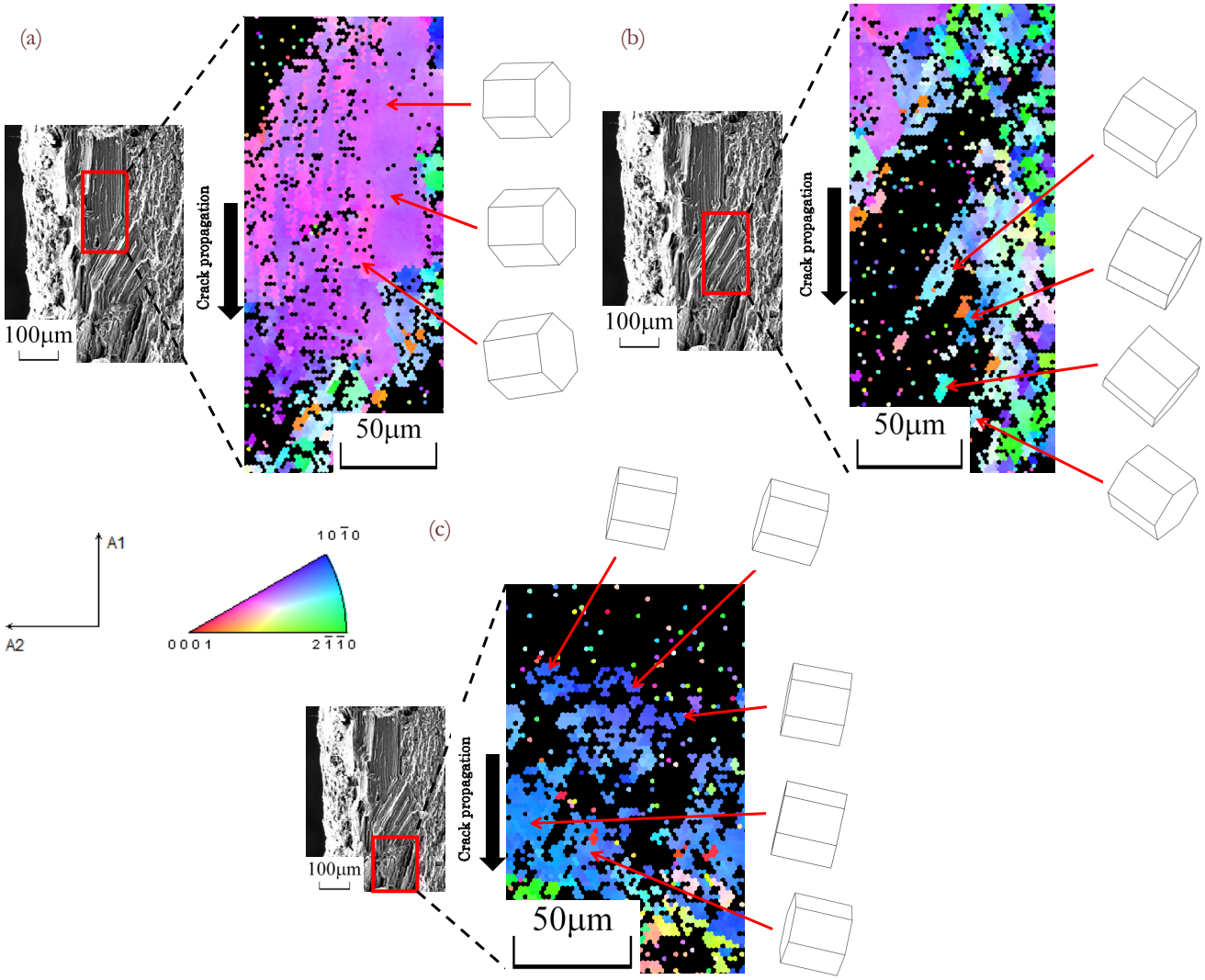

Figure 5: EBSD assisted fractography; (a) Area I, (b) Area II, (c) Area III.

Twining is major deformation mechanism in Mg alloy with relatively low CRSS, and generally observed as twin band in the EBSD analysis. Especially in the area "I" (Fig.5(a)), the area with high CI values is relatively large. But twin band was not recognized in this area, indicating that basal slip predominantly operated. Based on the Euler angle of the grain, Schmid factor and angle analyses were performed. As schematically seen in Fig.6, the coordinate A1, A2 and A3 in EBSD analysis was fixed against fractured CT specimen (Fig.6(a)). When the slip plane in Fig.6(b) operated, the intersection line between slip plane and A1-A2 plane (fracture surface) could be defined as a slip line. Then, the angle, α, was defined as the angle between slip line and specimen thickness direction. Plus or minus sign of α was defined as shown in Fig.6(c). The typical examples of Schmid factors and the angles calculated in the area "I" (Fig.5(a)) and "III" (Fig.5(c)) are summarized in Tabs. 1 and 2, respectively. For example, when basal slip operated in the area "I", the calculated angle, α, is -86.74° (Tab. 1), indicating that the slip line should nearly parallel to the crack propagation direction on the fracture surface. In Fig.5(a), the lines are nearly parallel to the crack propagation direction as predicted from Euler angle. Furthermore, twining is hardly seen in the area "I". Consequently, it could be concluded that the parallel lines in the area "I" were formed due to the operation of basal slip. It should be noted that basal slip systems (0001)[11-20] and (0001)[1-210] have high Schmid factors, indicating that those slip systems operated. In the area "III", the basal slip line angle, α, would be 75.73°, which corresponds well with the actual angles of parallel lines in (Fig.5(c)), namely 80°. The angles of

primary twin planes are largely different from 80º, and twining was not observed in the area "III", indicating those parallel lines were formed due to basal slip operation.

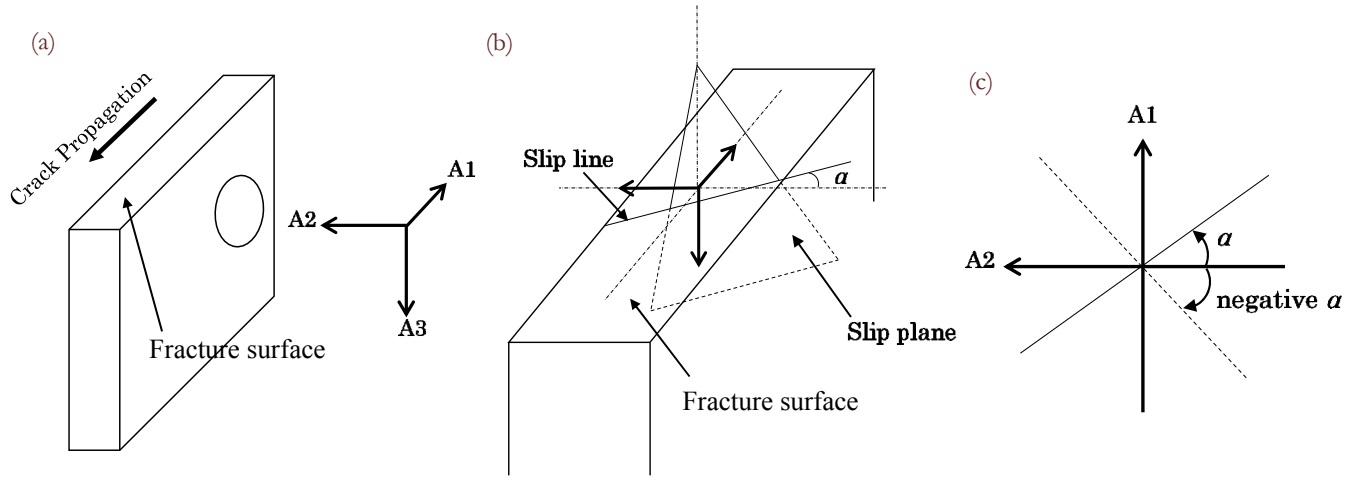

Figure 6: Schematic illustration of angle analysis; (a) Coordinates, (b) Definition of angle, α, (c) Definition of Plus or minus sign of α.

	Slip plane	Slip direction	Schmid factor	Slip angle, α
Basal slip	(0001)	[11-20]	0.38	-86.74
		[2-1-10]	-0.02	
		[1-210]	-0.40	
Primary twin	(01-12)	[01-1-1]	-0.19	-89.18
	(10-12)	[10-1-1]	-0.31	-51.89
	(1-102)	[1-10-1]	0.33	-33.51
	(0-112)	[0-11-1]	0.25	-77.52
	(-1012)	[-101-1]	-0.34	39.57
	(-1102)	[-110-1]	0.30	55.16

Table 1: Schmid factors and slip angles calculated in the area "I" in Fig.4(a).

	Slip plane	Slip direction	Schmid factor	Slip angle, α
Basal slip	(0001)	[11-20]	-0.26	75.73
		[2-1-10]	-0.15	
		[1-210]	0.11	
Primary twin	(01-12)	[01-1-1]	-0.45	33.48
	(10-12)	[10-1-1]	-0.45	41.87
	(1-102)	[1-10-1]	0.46	-85.29
	(0-112)	[0-11-1]	0.42	-60.89
	(-1012)	[-101-1]	-0.42	-74.55
	(-1102)	[-110-1]	0.46	60.02

Table 2: Schmid factors and slip angles calculated in the area "III" in Fig.4(c).

Fatigue crack propagation (FCP) under the cathodic potential of -3V

Fig. 7 shows the fracture surface of FCP test under the cathodic potential of -3V [7]. As shown in the figure, parallel lines are recognized on the fracture surface at ΔK=3.6MPam$^{1/2}$. Based on the similar procedure in the preceding section, EBSD-assisted fractography was performed on the FCP fracture surface as shown in Fig.7. EBSD result in Fig.7 is showing the area with high CI values. First, it should be noted that twin band is hardly seen in this area. Secondly, Schmid factor and angle analysis results are summarized in Tab. 3, showing the calculated slip plane angle is 71.25°. The actual angle of parallel lines is 70 as shown in Fig.7. Consequently, it could concluded that the parallel lines were formed do to the operation of basal slip. It should be noted that the slip system (0001)[1-210] with the highest Schmid factor might have operated.

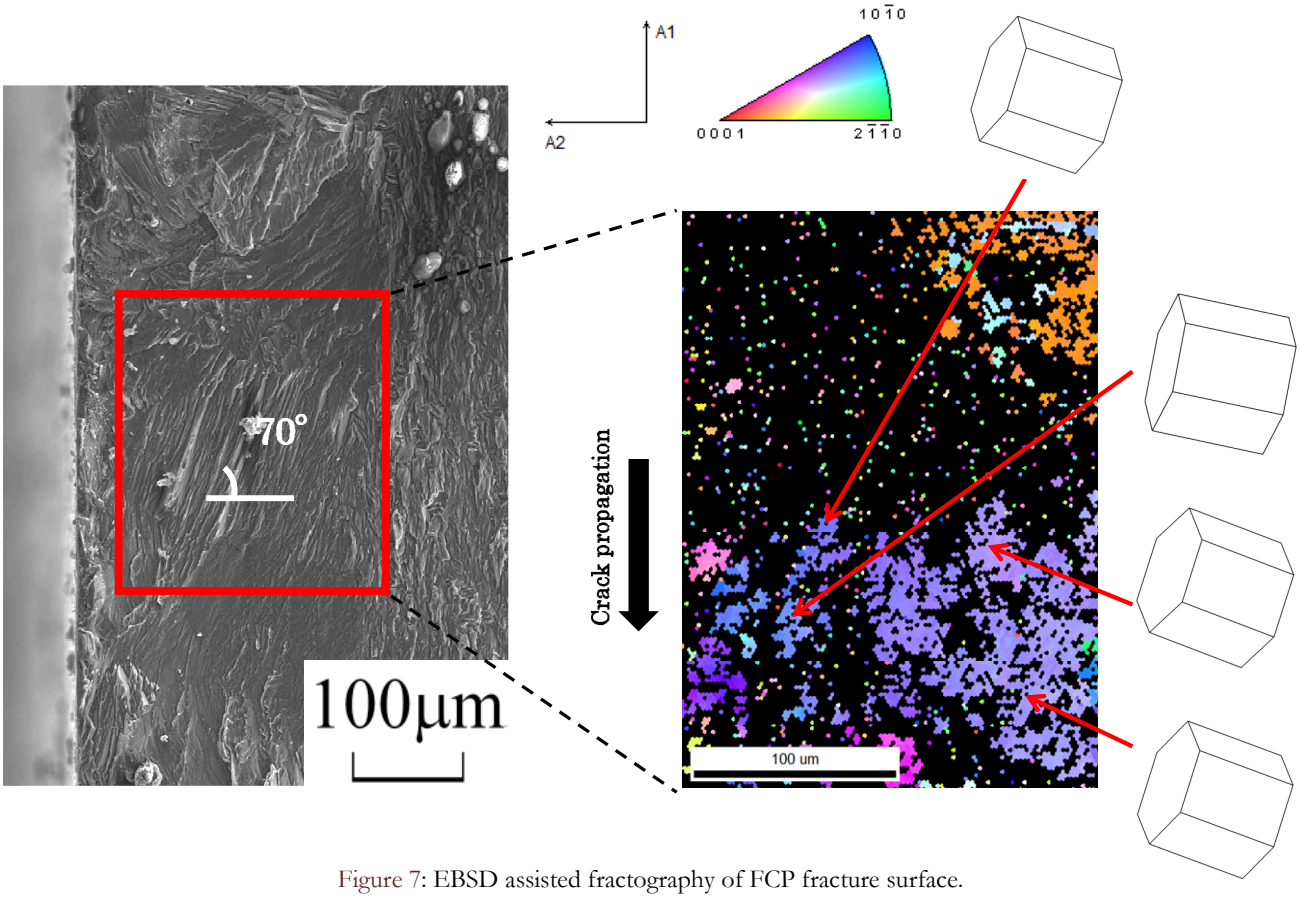

Figure 7: EBSD assisted fractography of FCP fracture surface.

	Slip plane	Slip direction	Schmid factor	Slip angle, α
Basal slip	(0001)	[11-20]	-0.14	
		[2-1-10]	0.25	71.25
		[1-210]	0.39	
Primary twin	(01-12)	[01-1-1]	-0.36	60.89
	(10-12)	[10-1-1]	-0.39	-64.24
	(1-102)	[1-10-1]	0.29	-69.68
	(0-112)	[0-11-1]	0.32	76.60
	(-1012)	[-101-1]	-0.40	37.80
	(-1102)	[-110-1]	0.34	24.96

Table 3: Schmid factors and slip angles calculated in the area in Fig.7.

The parallel lines are generally formed on the fracture surfaces when SCC or FCP occurred under hydrogen charged conditions [4-7]. However, FCP fracture surface in dry air did not show those parallel lines. Thus it is considered that hydrogen charging is related to the formation of parallel lines. As mentioned above, parallel lines were formed due to the operation of basal slip lines, implying that basal slip operation was enhanced by hydrogen charging. It has been proposed that the local plasticity was enhanced by hydrogen charging in steel materials, which is known as hydrogen-enhanced localized plasticity (HELP) model [8]. In the HELP model, it is considered that the stress distribution induced by the solubility of hydrogen would result in the enhancement of dislocation mobility. Consequently, it is considered that HELP had operated even in Mg alloy and resulted in the formation of characteristic parallel lines in the fracture surfaces under hydrogen charged conditions.

CONCLUSION

Stress corrosion cracking (SCC) and fatigue crack propagation (FCP) fracture surfaces in AZ61 Mg alloy under hydrogen charged conditions were analyzed based on EBSD-assisted fractography. The conclusions are as follows.

(1) Characteristic parallel lines were formed on the SCC and FCP fracture surfaces under hydrogen charged conditions, while the feature was not observed on the fracture surfaces of FCP in dry air.

(2) EBSD-assisted fractography revealed that the parallel lines were formed due to the operation of basal slip systems. Twining was not recognized on the fracture surfaces. It is considered that the basal slip was activated under hydrogen charged condition.

(3) Hydrogen-enhanced localized plasticity (HELP), known in steels, might have operated in Mg alloy.

REFERENCES

[1] Songa, R.G., Blawert, C., Dietzel, W., Atrens A., A study on stress corrosion cracking and hydrogen embrittlement of AZ31 magnesium alloy, Mater. Sci. Eng., A399 (2005) 308-317.

[2] Winzer, N., Atrens, A., Dietzel, W., Raja, V.S., Song, G., Kainer, K.U., Characterisation of stress corrosion cracking (SCC) of Mg–Al alloys, Mater. Sci. Eng., A488 (2008) 339-351.

[3] Kannan, M.B., Singh Raman, R.K., Evaluating the stress corrosion cracking susceptibility of Mg–Al–Zn alloy in modified-simulated body fluid for orthopaedic implant application, Scripta Materialia, 29 (2008) 175-175.

[4] Uematsu, Y., Kakiuchi, T., Nakajima, M., Stress corrosion cracking behavior of the wrought magnesium alloy AZ31 under controlled cathodic potentials, Mater. Sci. Eng., A531 (2012) 171-177.

[5] Kakiuchi, T., Uematsu, Y., Nakajima, M., Nakamura, Y., Miyagi, K., Stress corrosion cracking behavior of wrought magnesium alloy AZ31 and AZ61 under controlled cathodic potentials, Proc., 13th Int. Conf. on Fracture (ICF13), Beijing, China, 2013.

[6] Tokaji, K., Nakajima, M., Uematsu, Y., Fatigue crack propagation and fracture mechanisms of wrought magnesium alloys in different environments, Int. J. Fatigue, 31-7 (2009) 1137-1143.

[7] Uematsu, Y., Kakiuchi, T., Nakajima, M., Nakamura, Y., Miyazaki, S., Makino, H., Fatigue crack propagation of AZ61 magnesium alloy under controlled humidity and visualization of hydrogen diffusion along the crack wake, Int. J. Fatigue, 59-2 (2014) 234-243.

[8] Birnbaum, H.K., Sofronis, P., Hydrogen-enhanced localized plasticity—a mechanism for hydrogen-related fracture, Mater. Sci. Eng., A176 (1994) 191-202.